Biomaterials 271 (2021) 120754

Contents lists available at ScienceDirect

Biomaterials

journal homepage: www.elsevier.com/locate/biomaterials

The organometallic ferrocene exhibits amplified anti-tumor activity by targeted delivery via highly selective ligands to αvβ3, αvβ6, or α5β1 integrins

Beatrice Stefanie Ludwig [a,b], Stefano Tomassi [c], Salvatore Di Maro [d], Francesco Saverio Di Leva [c], Anke Benge [e], Florian Reichart [f], Markus Nieberler [g], Fritz E. Kühn [h,i], Horst Kessler [f], Luciana Marinelli [c], Ute Reuning [e,1], Susanne Kossatz [a,b,i,*,1]

[a] Department of Nuclear Medicine, University Hospital Klinikum rechts der Isar, Technical University Munich, Munich, Germany
[b] Central Institute for Translational Cancer Research (TranslaTUM), Technical University of Munich, Munich, Germany
[c] Department of Pharmacy, University of Naples "Federico II", Naples, Italy
[d] Università degli Studi della Campania "Luigi Vanvitelli", Department of Environmental, Biological and Pharmaceutical Sciences and Technologies, Caserta, Italy
[e] Department of Obstetrics and Gynecology, Clinical Research Unit, University Hospital Klinikum rechts der Isar, Technical University Munich, Munich, Germany
[f] Institute for Advanced Study, Department of Chemistry, Technical University Munich, Garching, Germany
[g] Department of Oral and Maxillofacial Surgery, University Hospital Klinikum rechts der Isar, Technical University Munich, Munich, Germany
[h] Molecular Catalysis, Catalysis Research Center, Technical University Munich, Munich, Germany
[i] Department of Chemistry, Technical University Munich, Munich, Germany

ARTICLE INFO

Keywords:
Targeted drug delivery
Synthetic integrin ligands to αvβ3
αvβ6
α5β1
Reactive oxygen species
Tumor cell cytotoxicity
Ferrocene

ABSTRACT

High levels of reactive oxygen species (ROS) in tumors have been shown to exert anti-tumor activity, leading to the concept of ROS induction as therapeutic strategy. The organometallic compound ferrocene (Fc) generates ROS through a reversible one-electron oxidation. Incorporation of Fc into a tumor-targeting, bioactive molecule can enhance its therapeutic activity and enable tumor specific delivery. Therefore, we conjugated Fc to five synthetic, *Arg-Gly-Asp* (RGD)-based integrin binding ligands to enable targeting of the cell adhesion and signaling receptor integrin subtypes αvβ3, α5β1, or αvβ6, which are overexpressed in various, distinct tumors. We designed and synthesized a library of integrin-ligand-ferrocene (ILF) derivatives and showed that ILF conjugates maintained the high integrin affinity and selectivity of their parent ligands. A thorough biological characterization allowed us to identify the two most promising ligands, an αvβ3 (L2b) and an αvβ6 (L3b) targeting ILF, which displayed selective integrin-dependent cell uptake and pronounced ferrocene-mediated anti-tumor effects *in vitro*, along with increased ROS production and DNA damage. Hence, ILFs are promising candidates for the selective, tumor-targeted delivery of ferrocene to maximize its anti-cancer efficacy and minimize systemic toxicity, thereby improving the therapeutic window of ferrocene compared to currently used non-selective anti-cancer drugs.

1. Introduction

Targeted drug delivery holds the potential to increase the therapeutic index of non-targeted systemic drugs [1,2]. In this therapeutic concept, drugs can be attached to tumor-targeting vehicles that selectively interact with unique molecular targets of cancer cells, such as cell membrane receptors, which are lacking or only weakly expressed in healthy cells.

Among the promising candidates for targeted drug delivery approaches, integrins are a family of well-known transmembrane receptors, which mediate many important cellular processes, like adhesion, migration, invasion, proliferation, and survival. This class of receptors came into the limelight due to their involvement in numerous pathophysiological events, such as tumor progression and metastasis [3–7]. They are heterodimeric glycoproteins, non-covalently combining one out of 18 α- and one out of 8 β-subunits [8,9]. Among the 24

* Corresponding author. Ismaninger Straße 22, Munich, Germany.
E-mail address: s.kossatz@tum.de (S. Kossatz).
[1] contributed equally.

https://doi.org/10.1016/j.biomaterials.2021.120754
Received 28 October 2020; Received in revised form 17 February 2021; Accepted 8 March 2021
Available online 12 March 2021

different integrin subtypes known in mammals, eight bind their specific ligands via an RGD recognition motif [10]. These include αvβ3, αvβ6 and α5β1, which are overexpressed in various cancer types and are classified as valuable structures for selective tumor targeting [4,11,12]. Integrin αvβ3 is a pro-angiogenic factor, e.g. in invasive melanoma, neuroblastic tumors, and breast cancer, where its expression is upregulated and connected to invasive growth [4,13,14]. Integrin αvβ6 overexpression was described in pancreatic cancer, non-small cell lung cancer, and oral squamous cell carcinoma [4]. Integrin α5β1 overexpression was reported in glioblastoma multiforme, lung, and ovarian cancers [4, 15–17].

In the present study, we investigated the ability of several integrin subtype-selective ligands to promote specific delivery of the organometallic sandwich molecule ferrocene (Fc) to tumor cells overexpressing a distinct integrin species. Fc as an organometallic is well known since its discovery in 1951 [18–20]. More recently, it has received a lot of interest in medicinal chemistry as a building block of novel drug candidates, where it exerts antitumoral, antifungal, antimalarial, and antiviral activity via a number of different mechanisms based on its versatile metal-based properties (recently reviewed in Refs. [21–25]). The most prominent examples are Ferrocifen [26], which is a Fc-containing derivative of the breast cancer therapeutic tamoxifen, as well as Ferroquine [27], a Fc-derivative of the anti-malaria drug chloroquine, which is currently evaluated in phase II clinical trials. The majority of Fc containing anti-tumor drug candidates incorporate Fc into a bioactive molecule, e.g. by replacing a phenyl ring, with the goal to enhance its cytotoxic potency or overcome drug resistance [23,28,29].

The cytotoxic activity of Fc is - among other mechanisms - mediated through its ability to provoke the generation of reactive oxygen species (ROS), based on its redox potential (+0.40 V), which is compatible with intracellular redox potentials ranging from +0.40 V to −0.44 V [30]. Therefore, Fc undergoes electron transfer reactions and redox cycling within a cell [30]. Fc (Fe-II) reacts through a reversible one-electron oxidation via a *Fenton*-like reaction to a ferrocenium cation Fc^+ (Fe-III), thereby generating •OH and concomitantly ROS [23], which in turn induce DNA cleavage [31] and cell death. The anti-tumor activity of Fc itself is low [32] due to hampered intracellular translocation as well as poor water solubility [33]. Analyses of the therapeutic potential of Fc without incorporation into an already cytotoxic compound or chemical modification of its water solubility are scarce (recently reviewed in Refs. [21,24]).

Here, we propose a strategy, where Fc is conjugated to integrin binding peptides and peptidomimetics, which display excellent tumor-targeting properties but lack inherent therapeutic activity. By targeting cell surface receptors, which are overexpressed in tumors and are internalized following ligand binding, we aimed at focusing on the anti-tumor effect of Fc itself by increasing its intratumoral concentration and reducing unwanted cytotoxicity in benign cells that do not overexpress the receptor of interest. In addition, by addressing different tumor-biologically relevant integrins, we wanted to dissect the importance of subtype specificity of the respective integrin-targeting ligands.

The concept of targeting integrins with Fc has been previously addressed by Zhou et al. [34]. However, this study used a tripeptide RGD, which was not characterized with respect to its integrin affinity or subtype selectivity. Importantly, the tripeptide RGD alone led to a pronounced reduction of cell viability, while our study was focused on integrin ligands which lack inherent cytotoxic activity.

We synthesized a library of integrin-ligand ferrocene conjugates (ILFs) and explored their ability to target tumor cells that express elevated levels of the integrin subtypes αvβ3, αvβ6 or α5β1. We demonstrated that ILFs enabled integrin subtype specific intracellular Fc delivery, boosting Fc-mediated tumor cytotoxic effects compared to the low cytotoxic activity of free Fc-COOH. We provide an in-depth analysis of their integrin selectivity, affinity, cell binding/uptake, and tumor cell killing potential concomitant with increases in ROS levels and DNA damage.

2. Materials and methods

Chemicals and cell culture materials. Unless otherwise noted, all reagents, solvents, and resins were obtained from commercial suppliers, of analytical, "for synthesis", peptide or HPLC grade and used without further purification. Peptides of the L4 series (L4H, L4a-c) were assembled using a Macherey-Nagel Chromab. vacuum manifold and an ultrasonic bath *SONOREX* RK 52H (interior dimensions 150 × 140 × 100 mm and operating volume 1.2 L) by BANDELIN electronic (Mörfelden-Walldorf, Germany). Saturated solutions were aqueous solutions. 3-(4,5-dimethylthiazol-2-yl)-2,5-diphenyltetrazolium bromide (MTT) was purchased from Sigma-Aldrich (St. Louis, USA). Trypsin-EDTA (10 ×), Dulbecco's Modified Essential Medium GlutaMAX™ (DMEM), Roswell Park Memorial Institute-1640 Medium (RPMI-1640), Minimum Essential Medium (MEM), fetal calf serum (FCS), and 1 × phosphate buffer saline (PBS; pH 7.4) were purchased from Gibco, Thermo Fisher Scientific (Waltham, USA).

Chromatography. Analytical high-pressure chromatography electrospray ionization-mass spectrometry (HPLC-ESI-MS) was performed on a UltiMate 3000 UHPLC (Dionex, Sunnyvale, USA) equipped with a LCQ Fleet mass spectrometer (Thermo Scientific) using a long C18 column ("S1", Hypersil Gold aQ 175 Å, 3 µm, 150 mm × 2.1 mm) or a short C18 column ("S2", Accucore C18, 80 Å, 2.6 µm, 50 × 2.1 mm) from Thermo Scientific. Linear gradients (0.9 mL/min; 8 min, S1 or 5 min, S2) of H_2O (0.1% (v/v) formic acid) and acetonitrile (MeCN; 0.1% (v/v) formic acid) were used for analytical purpose. All final compounds were analyzed via analytical HPLC to confirm a purity of ≥95% (220 nm). Semi-preparative reversed phase HPLC was performed using a Waters (Milford, USA) instrument including a Waters 2545 (Binary Gradient Module), Waters SFO (System Fluidics Organizer), Waters 2996 (Photodiode Array Detector), and Waters 2767 (Sample Manager). Suitable linear gradients of H_2O (0.1% (v/v) trifluoroacetic acid (TFA), buffer A) and MeCN (0.1% (v/v) TFA, buffer B) were applied for the purification of all compounds using (unless otherwise noted) a C18-column (Reprosil 100C18, 5 µm, 150 × 30 mm, Dr. Maisch, Ammerbuch-Entringen, Germany) with a flow rate of 40 mL/min. Column chromatographic separations were carried out with a 100-fold mass excess of silica gel (40–63 μm, Si 60, 230–400 mesh ATSM, Merck Millipore, Burlington, USA) at 1 bar overpressure. The peptides of the L4 (L4H, L4a-c) series were purified by preparative HPLC (Shimadzu HPLC system) equipped with a C18-bounded preparative RP-HPLC column (Phenomenex (Torrance, USA) Kinetex 21.2 mm × 150 mm, 5 µm). Peptides were analyzed by analytical HPLC (Shimadzu (Kyoto, Japan) Prominance HPLC system) equipped with a C18-bounded analytical RP-HPLC column (Phenomenex Kinetex, 4.6 mm × 150 mm, 5 µM) using a gradient elution (from 10 to 90% (v/v) acetonitrile in water (0.1% (v/v) TFA) over 20 min; flow rate = 1.0 mL/min; diode array UV detector). Molecular weights of compounds were confirmed by ESI-MS (LTQ-XL Thermo Fisher Scientific).

Nuclear Magnetic Resonance (NMR) spectroscopy. ^{1}H-NMR and ^{13}C-NMR spectra were recorded at 298 K on a 400 MHz AV spectrometer and on a 300 MHz AV spectrometer from Bruker (Billerica, USA). Chemical shifts are given in *parts per million* (ppm). Internal standards for the chemical shifts of ^{1}H and ^{13}C were the following solvent signals: $CDCl_3$: 7.26 ppm (^{1}H-NMR) and 77.16 ppm (^{13}C-NMR); DMSO-d_6: 2.50 ppm (^{1}H-NMR) and 39.52 ppm (^{13}C-NMR). Abbreviations for NMR signal multiplicities are: singlet (s), doublet (d), triplet (t), quartet (q), multiplet (m). Coupling constants J are given in Hz as mean values of experimentally determined values. The data were processed and evaluated using the program *MestreNova* (version 9.0).

Chemical synthesis. The detailed experimental procedures for the generation of the integrin ligands and their conjugation to Fc (**see Fig. 1**) can be found in the Supporting Information 1, Chemical synthesis methods, and figures.

Integrin binding affinity assay. The affinity and selectivity of the ILF derivatives and the integrin ligands were determined via a solid-phase

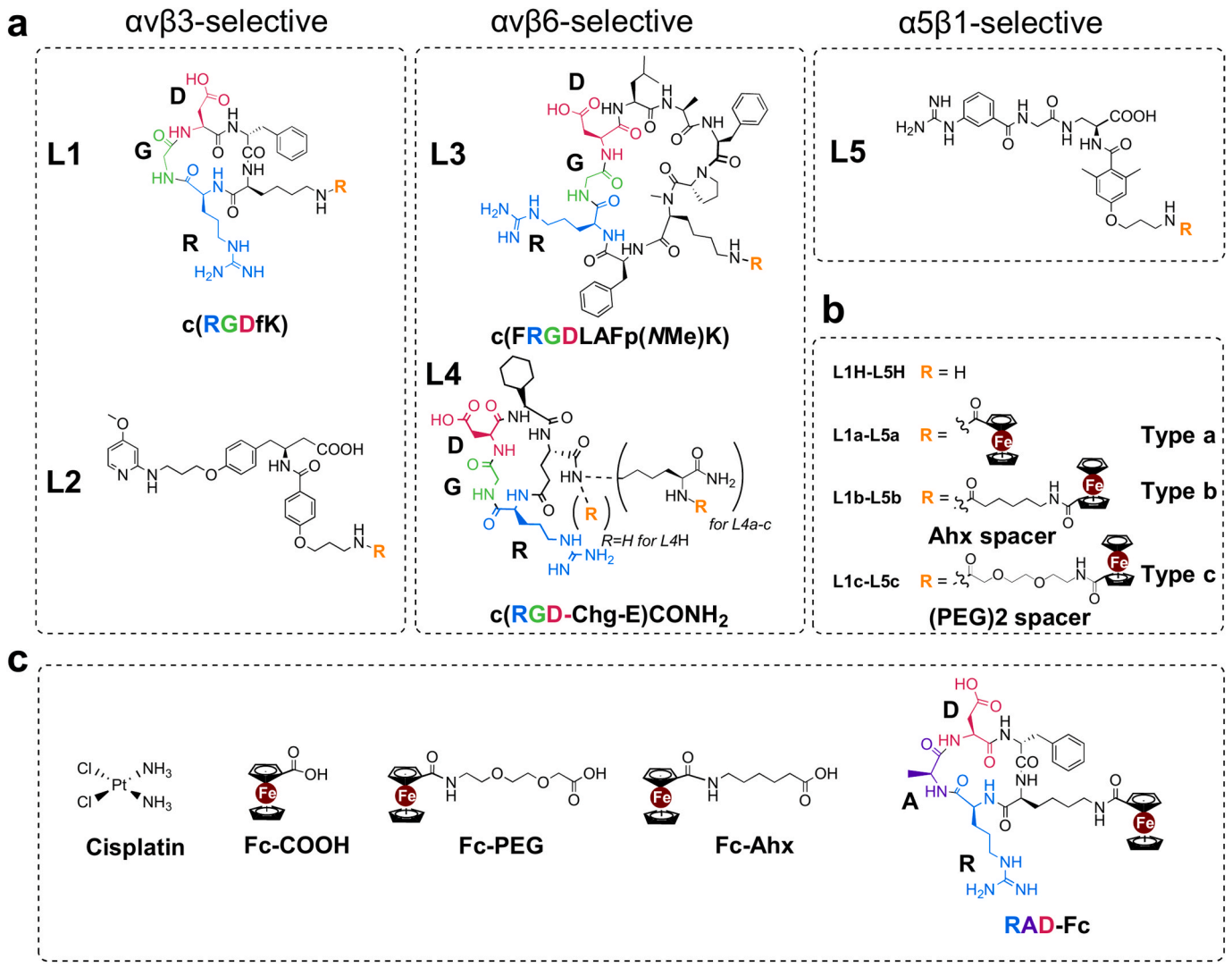

Fig. 1. Chemical structures of synthesized ILF derivatives. (a) Five different selective peptidic or peptidomimetic integrin ligands targeting αvβ3, αvβ6, or α5β1 were chosen for conjugation to Fc. (**b**) Conjugation occurred either directly to Fc-COOH (L1a-L5a) or via a spacer unit (Ahx-spacer: L1b-L5b, or $(PEG)_2$-spacer: L1c-L5c). As controls, unconjugated integrin ligands were generated (L1H-L5H). In case of L4-derivatives, Fc with and without linkers was connected to the ligand through an additional lysine spacer. **(c)** The negative controls are Fc-COOH, Fc-$(PEG)_2$, Fc-Ahx, and the non-integrin-binding peptide RAD-Fc. Cisplatin was chosen as cytotoxic, non-selective control compound.

binding assay by applying a previously described protocol [35,36] that involves coated extracellular matrix (ECM) proteins and soluble integrins. The following compounds were used as internal standards: **Cilengitide** [37] c(RGDf(*N*Me)V) (reference values for: αvβ3 – 0.54 nM, α5β1 – 15.4 nM) and the linear peptide **RTDLDSLRT** [38] (reference value for: αvβ6 – 33 nM). First, flat-bottomed 96-well ELISA plates (BRAND) were coated overnight at 4 °C with the **ECM protein (1)** (100 μL/well) in carbonate buffer (15 mM Na_2CO_3, 35 mM $NaHCO_3$, pH 9.6). Afterwards, each well was washed with PBS-T buffer (phosphate--buffered saline/0.01% (v/v) Tween 20, 137 mM NaCl, 2.7 mM KCl, 10 mM Na_2HPO_4, 2 mM KH_2PO_4, pH 7.4; 3 × 200 μL) and blocked for 1 h at room temperature (RT) with TS-B buffer (Tris-saline/bovine serum albumin (BSA) buffer, 20 mM Tris-HCl, 150 mM NaCl, 1 mM $CaCl_2$, 1 mM $MgCl_2$, 1 mM $MnCl_2$, 1% (w/v) BSA, pH 7.5; 150 μL/well). Meanwhile, dilution series of the compounds and the internal standards were prepared in an extra plate, ranging from 20 μM to 256 pM in 1:5 dilution steps. After washing the assay plate three times with PBS-T (200 μL), 50 μL of the dilution series were transferred to each well from B-G in 6 appropriate concentrations. Hereby, well A was filled with 100 μL of TS-B solution (blank), and well H was filled with 50 μL of TSB buffer. Then, 50 μL of a solution of **human integrin (2)** in TS-B buffer was transferred to wells H–B and incubated for 1 h at RT. The plate was washed three times with PBS-T buffer, followed by the addition of the **primary antibody (3)** (100 μL/well). After incubation for 1 h at RT, the plate was washed three times with PBS-T (200 μL/well). Subsequently, a **secondary peroxidase-conjugated antibody (4)** (100 μL/well) was added to the plate and incubated for 1 h at RT. After washing the plate three times with PBS-T (200 μL/well), the plate was developed by quick addition of *SeramunBlau* (50 μL/well, Seramun Diagnostic GmbH) and incubated for approximately 1–2 min at RT in the dark. The reaction was stopped with 3 M H_2SO_4 (50 μL/well, quick addition), and the absorbance measured at 450 nm using a plate reader (Infinite M200 Pro, TECAN). The IC_{50} value (with 95% confidence interval) of each compound resulted from a sigmoidal fit of two data rows (serial dilution rows) done by *OriginPro 9.0G* statistical software. All IC_{50} values were referenced to the affinity of the internal standard.

For the integrin binding assay, the following integrins, antibodies and ECM proteins were used: **integrin αvβ3: (1)** 1.0 μg/mL human vitronectin (Merck Millipore, #CC080), **(2)** 2.0 μg/mL human αvβ3-integrin (R&D, #3050-AV-050). **(3)** 2.0 μg/mL mouse anti-human CD51/61 (BD Biosciences, #555504). **(4)** 2.0 μg/mL anti-mouse IgG-POD (Sigma-Aldrich, #A9044-2 ML). **Integrin α5β1: (1)** 0.5 μg/mL;

human fibronectin (Sigma-Aldrich, #F0895-1 MG), **(2)** 2.0 μg/mL human α5β1-integrin (R&D, 3230-A5-050), **(3)** 1.0 μg/mL mouse anti-human CD49e (BD Biosciences, #555651), **(4)** 2.0 μg/mL anti-mouse IgG-POD (Sigma-Aldrich, #A9044-2 ML). **Integrin αvβ6: (1)** 0.4 μg/mL; LAP (Latency Associated Peptide-) (R&D, #246-LP-025), **(2)** 0.5 μg/mL human αvβ6-integrin (R&D, #3817-AV-050), **(3)** 1:500 dilution, anti-*αv* mouse anti-human MAB1978 (Merck Millipore, #MAB1978), **(4)** 2.0 μg/mL, anti-mouse IgG-POD (Sigma-Aldrich, #A9044-2 ML).

Cell culture. *Melanoma cell lines M21 and M21-L+*. M21 and M21-L+ were purchased from American Type Culture Collection (ATCC) and cultured in RPMI-1640 supplemented with 10% (v/v) heat inactivated fetal calf serum (FCS), 1% (v/v) HEPES and 0.2% (v/v) *Arg-Asp* ("culture medium") in a 37 °C incubator with 5% (v/v) CO_2 atmosphere. *Ovarian cancer cell line OV-MZ-6 and human oral squamous cell carcinoma cell lines HN and BHY*. HN and BHY cell lines were purchased from the German Collection of Microorganisms and Cell Cultures (DSMZ nos. ACC 417 and ACC 404, respectively). HN cells were established from a cervical lymph node metastasis of a highly aggressive and invasive squamous cell carcinoma of the soft palate. The cells were cultured in DMEM supplemented with 10% (v/v) heat inactivated FCS, 1% (v/v) HEPES and 0.2% (v/v) *Arg-Asp* in a 37 °C incubator with 5% (v/v) CO_2 atmosphere. OV-MZ-6 cells were isolated from ascites of a patient afflicted with a cystadenocarcinoma of the ovary and were kindly provided by V. Möbus [39]. *Colon carcinoma cell line RKO*. RKO cells were purchased from ATCC and cultivated in MEM supplemented with 10% (v/v) heat inactivated FCS and 1% (v/v) HEPES ("culture medium") in a 37 °C incubator with 5% (v/v) CO_2 atmosphere.

Immunocytochemical detection of integrins αvβ3, αvβ6, and α5β1. Microchamber cell culture slides (Sarstedt) were coated with fibronectin (Corning, 2 μg/mL in PBS; 300 μL/well, 30 min at RT) and cells seeded at a density of 40000 cells/well. After 24 h of cultivation, cells were fixed with 4% (w/v) paraformaldehyde (PFA; 300 μL/well) in PBS for 20 min at RT. Subsequently, the cells were washed with PBS (2 × 800 μL), and blocked with 2% (w/v) bovine serum albumin (BSA; 500 μL/well) in PBS for 1 h at RT. The monoclonal primary antibody (1) (150 μL/well) in 1% (w/v) BSA/PBS was added to the cells, following incubation for 2 h at RT. Cells without primary antibody were treated with 1% (w/v) BSA/PBS (150 μL/well). After washing the cells three times with PBS (3 × 800 μL), a secondary, Alexa-568-conjugated antibody (2) (300 μL/well) was added and incubated with the cells for 45 min at RT in the dark. Thereafter, cells were washed repeatedly with PBS and mounted in PBS for subsequent fluorescence analysis using a Zeiss LSM 700 confocal microscope (Zeiss, Jena, Germany).

For the experiment, the following antibodies were used: **αvβ3-ICC: (1)** 1:100 dilution, mouse anti-human *αvβ*3 integrin monoclonal antibody, isotype IgG1, clone 23C6 (stock solution: 1 mg/mL, Merck Millipore, #CBL544), (2) 1:1000 dilution, goat-anti-mouse IgG (H + L) (stock solution: 2 mg/mL, Invitrogen, #A11004). **α5β1-ICC: (1)** 1:100 dilution, rabbit anti-human α5β1 integrin monoclonal antibody, isotype IgG-κ, clone M200/Volociximab (stock solution: 1 mg/mL, NovusBiologicals, Littleton, USA, #NBP2-52680), (2) 1:1000 dilution, goat-anti-rabbit IgG (H + L) (stock solution: 2 mg/mL, Invitrogen, # A11011). **αvβ6-ICC: (1)** 1:3000 dilution, clone 6.2A1 [40] (stock solution: 2 mg/mL, provided by Paul H. Weinreb, Biogen, München, Germany), (2) 1:1000 dilution, goat-anti-mouse IgG (H + L) (stock solution: 2 mg/mL, Invitrogen, # A11004).

Cellular uptake of Cy5.5-labeled integrin ligands. Microchamber cell culture slides were coated with fibronectin as described above, followed by cell seeding at a density of 50000 cells/well. After a cultivation period of 24 h, cells were treated with integrin ligands L1-Cy5.5 to L5-Cy5.5 (1 μM in 0.01% (w/v) $CaCl_2$ and 0.1% (w/v) BSA in PBS; 250 μL/well) for 40 min in the cell incubator. The cells were washed with PBS/0.01% (w/v) $CaCl_2$ (6 × 800 μL) and the fluorescence signal intensity recorded using a Zeiss LSM 700. In order to convert the fluorescence staining intensity into colors of a glow scale, the look-up table "orange-to-white" provided with the LSM scanning software Zen (Zeiss) was applied: low intensity (dark orange), medium intensity (yellow), and high intensity (white). Hoechst 33342 (Thermo Fisher Scientific) was used to stain cell nuclei.

Determination of cell viability. Cells were seeded in 96-well cell culture plates at 3500 cells/well, and cultured for 24 h at 37 °C. The culture medium was removed, and new culture medium containing the ILF derivatives, the unconjugated L1H-L5H integrin binding ligands, the negative controls (concentrations: 0 μM, 10 μM, 50 μM, 100 μM, 500 μM, 1000 μM, 70 μL/well), or cisplatin (0,1 μM, 1 μM, 20 μM, 70 μM, 200 μM) was added. After 24 h of incubation at 37 °C, a filtered solution of MTT (14 μL/well; 5 mg/mL in PBS) was added into each well. The cells were further incubated at 37 °C for 3 h. The MTT medium mixture of each well was carefully removed and replaced with DMSO (dimethyl sulfoxide, 150 μL/well). After 15 min in the cell incubator, the plates were gently agitated to completely dissolve all blue formazan crystals. With a plate reader (Multiskan™ Fc Photometer, Thermo Fisher Scientific) the absorbance was measured at 570 nm. The GI_{50} values (50% growth inhibition) were calculated using the *GraphPad Prism 8* software using non-linear regression (log (inhibitor) vs. normalized response).

Detection of reactive oxygen species (ROS). HN, M21, and OV-MZ-6 cells were seeded at a density of 50–60000 cells/well in a fibronectin-coated microchamber cell culture slide, and cultured for 24 h at 37 °C. Subsequently, the culture medium was removed, and the cells were washed with medium (2 × 800 μL/well). Then, new culture medium was added (500 μL/well) containing 20 μM of the test compound (L2b, L2H, L3b, L3H, RAD-Fc or Fc-COOH). In one well, cells were left without treatment (control: ROS production of untreated cells). The cells were incubated for 18 h at 37 °C before adding *CellROX*® (Thermo Fisher Scientific; 5 μM in medium; 200 μL/well), which was incubated for 30 min at 37 °C, followed by cell washes with 0.01% (w/v) $CaCl_2$ in PBS (4 × 800 μL) and mounting in PBS/$CaCl_2$ for fluorescence microscopy. Hoechst 33342 was used for nuclear counterstaining. The fluorescence signal intensity was recorded using the Zeiss LSM 700. ROS levels were quantified as mean fluorescence intensity per cell and normalized to untreated cells using the software *FIJI*.

Determination of DNA damage. Black, clear-bottom 96 well cell culture plates with cover-glass bottom (Nunclon™ Delta 96-Well MicroWell™ Plates, Thermo Fisher Scientific) were coated with fibronectin as described. HN cells were seeded at a density of 11000 cells/well and M21 and OV-MZ-6 cells at 9000 cells/well and cultured for 24 h at 37 °C. Subsequently, the culture medium was removed and the cells washed with medium (2 × 200 μL/well). Then, new culture medium was added (200 μL/well) containing 20 μM L2b, L2H, L3b, L3H RAD-Fc or Fc-COOH. Cells without treatment served as control. The cells were incubated for 18 h at 37 °C, afterwards fixed with 4% (w/v) PFA in PBS (150 μL/well, 10 min at RT) and permeabilized with 0.1% (v/v) Triton™-X100 in PBS (150 μL/well, 10 min at RT). After washing the cells with PBS (3 × 5 min), they were blocked with 3% (w/v) BSA (150 μL/well) in PBS for 1 h at RT. The primary antibody (1:500, 150 μL/well; phospho-histone H2A.X (Ser139) monoclonal antibody (GT2311) (Thermo Fisher Scientific, MA5-27753) was added in PBS containing 0.1% (v/v) Tween-20 and 3% (w/v) BSA and incubated for 1 h at RT. After washing the cells three times with PBS (3 × 200 μL), a secondary, AlexaFluor-488-conjugated goat-anti-rabbit IgG (H + L) (1:2000, 200 μL/well, Thermo Fisher Scientific, A11001) was added in 3% (w/v) BSA/PBS-T and incubated for 1 h at RT in the dark. Then, the cells were washed repeatedly with PBS and imaged using an EVOS M7000 microscope (Thermo Fisher Scientific), equipped with filter cubes to record Hoechst and AlexaFluor-488 fluorescence. We imaged at least 100 cells per condition and analyzed them for the number of γH2AX foci per cell using the Software *CellProfiler* and the "Speckle counting" pipeline.

Evaluation of ILF stability. The serum stability of ILF was analyzed by adapting a reported protocol [41]. 90 μL FCS was mixed with 10 μL of an aqueous solution of the ILF derivative (2 mM) and incubated at 37 °C 30 μL aliquots were collected at different time points (0, 0.5, 1, 6, 24 h). After precipitation with 30 μL MeCN/0.1% (v/v) TFA solution and

centrifugation (14000 rpm, 30 min, 4 °C), the supernatant was recovered and analyzed by HPLC-ESI-MS using a linear elution gradient from 5 to 95% (v/v) MeCN/0.1% (v/v) TFA in water/0.1% (v/v) TFA for 5 min. The results are depicted in the Supplementary Figure Section (Figure S55-S56) and in the Supplementary Table Section (Table ST1).

3. Results and discussion

3.1. Synthesis of ILF conjugates

In order to generate an ILF library, we chose, among our previously published ligands, five highly affine and selective ligands for the RGD recognizing integrins αvβ3 (peptidic L1 [42–45] and peptidomimetic L2 [46–48]), αvβ6 (peptidic L3 [49] and L4 [50]), and α5β1 (peptidomimetic L5 [48,51]) (Fig. 1a), which were synthesized using previously established protocols (**Supplementary Schemes SS1-SS4**; **Supplementary figures S1-47**).

For integrin ligand conjugation to Fc, we conceptualized three different derivatives for each ligand: i) direct attachment of ferrocene carboxylic acid (Fc-COOH) (*type a*; L1a-L5a), ii) introduction of a lipophilic spacer (aminohexanoic acid (Ahx), *type b*; L1b-L5b), or iii) a hydrophilic spacer (polyethylenglycol ($(PEG)_2$), *type c*; L1c-L5c) inserted between the Fc-moiety and the integrin ligand (Fig. 1b). In case of L4-derivatives, Fc with and without linkers was connected to the ligand through an additional lysine spacer. In all cases, Fc-COOH was conjugated to the amino-functionalized integrin ligands using standard peptide chemistry [23,52]. Different spacers were explored and evaluated for their impact on integrin ligand affinity and specificity and for optimal delivery of Fc to tumor cells. As controls, we synthesized the unconjugated parent integrin ligands L1H-L5H (Fig. 1a and b) as well as Fc-Ahx, Fc-$(PEG)_2$, and the non-integrin-binding peptide *Arg-Ala-Asp* (RAD)-Fc [44] (Fig. 1c). Thus, 23 different compounds with yields ranging between 3 and 32% and purities greater than 97% were generated (**Supplementary Figures S1-S47**).

3.2. Characterization of ILF-conjugates

We assessed integrin binding affinity and subtype selectivity for all ILFs and control compounds by an established solid-phase binding enzyme-linked immunosorbent assay (ELISA) that involves coated ECM proteins and purified soluble integrin species (Fig. 2, Table 1) [35,36,53]. As internal standard ligands, we used Cilengitide, c(RGDf(*N*Me)V) (reference IC_{50}-values: αvβ3 – 0.54 nM, α5β1 – 15.4 nM) and the linear peptide RTDLDSLRT ("RTD-lin") (reference IC_{50}-values: αvβ6 – 29.5 nM) [37,38].

Within the group of αvβ3 targeting ligands (L1, L2-based), αvβ3 affinity remained comparable (<20 nM) for all ILFs, and was two orders of magnitude higher than for αvβ6 and α5β1, respectively. Within the L1-series, all ligands demonstrated IC_{50} values in the low nM range (IC_{50}: 3–19 nM) towards αvβ3, which were comparable to the unconjugated control L1H (IC_{50}: 2 nM). For the L2 series, the αvβ3 IC_{50} values were even lower (IC_{50}: 0.9–1.3 nM) in comparison to the L1-derivates. This is likely due to the ligand binding properties, since L2 represents a peptidomimetic ligand, derived through rational design and computational docking studies to perfectly fit into the integrin binding pocket [46–48].

Table 1
Binding affinities of unconjugated integrin ligands L1H-L5H (grey), Fc-derivatives L1a-L5c, and negative controls Fc-COOH, Fc-Ahx, Fc-$(PEG)_2$, RAD-Fc for αvβ3, αvβ6, and α5β1, respectively. Selectivity profile of the ligands for RGD recognizing integrins were derived from a competitive ELISA assay.

Compound		IC_{50} αvβ3 [nM][a]	IC_{50} α5β1 [nM][a]	IC_{50} αvβ6 [nM][a]
αvβ3-selective ligands				
L1H[b]		2.24 ± 0.34	55 ± 9	141 ± 15
L1a	(Fc-no linker)	19.6 ± 6.05	>1000	113 ± 10.3
L1b	(Fc-Ahx linker)	6.21 ± 8.17	267 ± 50.3	56 ± 3.54
L1c	(Fc-$(PEG)_2$ linker)	3.08 ± 0.77	91.0 ± 8.67	57 ± 4.59
L2H		0.47 ± 0.05	152 ± 36	>1000[b]
L2a	(Fc-no linker)	0.96 ± 0.21	80.0 ± 19.1	146 ± 11.1
L2b	(Fc-Ahx linker)	1.34 ± 0.35	82.7 ± 16.9	128 ± 7.69
L2c	(Fc-$(PEG)_2$linker)	1.03 ± 0.31	88.5 ± 28.5	114 ± 7.87
αvβ6-selective ligands				
L3H[b]		>1000	73 ± 6	0.28 ± 0.019
L3a	(Fc-no linker)	>1000	45 ± 2.55	2.23 ± 0.74
L3b	(Fc-Ahx linker)	>1000	251 ± 126	9.49 ± 1.66
L3c	(Fc-$(PEG)_2$ linker)	>1000	283 ± 44.2	1.19 ± 0.36
L4H[b]		364 ± 96	105 ± 11	1.3 ± 0.2
L4a	(Fc-no linker)	>1000	36.4 ± 6.85	0.08 ± 0.01
L4b	(Fc-Ahx linker)	>1000	188 ± 63.1	0.28 ± 0.06
L4c	(Fc-$(PEG)_2$ linker)	>1000	26.7 ± 4.65	0.23 ± 0.04
α5β1-selective ligands				
L5H		>1000	1.74 ± 0.26	433 ± 101[b]
L5a	(Fc-no linker)	>1000	0.32 ± 0.12	746 ± 49.8
L5b	(Fc-Ahx linker)	>1000	0.18 ± 0.042	69 ± 8.15
L5c	(Fc-$(PEG)_2$ linker)	357 ± 411	5.00 ± 0.24	155 ± 6.12
Controls				
Fc-COOH		>1000	>1000	>1000
Fc-Ahx		>1000	>1000	>1000
Fc-$(PEG)_2$		>1000	>1000	>1000
RAD-Fc		>1000	841 ± 151	>1000
RTDLDSLRT[b]		>1000	>1000	29.5 ± 4.5
Internal standard				
Cilengitide[b]		0.61 ± 0.06	14.9 ± 3.1	>1000

[a] The IC_{50} values were determined using a sigmoidal fit to 16 data points, obtained from two serial dilution rows and by referencing to the affinity of the internal standards Cilengitide or RTDLDSLRT.

[b] IC_{50} values of L1H [36], L3H [36], c(RGD-Chg-E)-$CONH_2$ [50] and *αvβ6* value for L2H [36] and L5H [36] (for ligand with isopropylgroup instead of free amine), Cilengitide [79] and RTDLDSLRT [36].

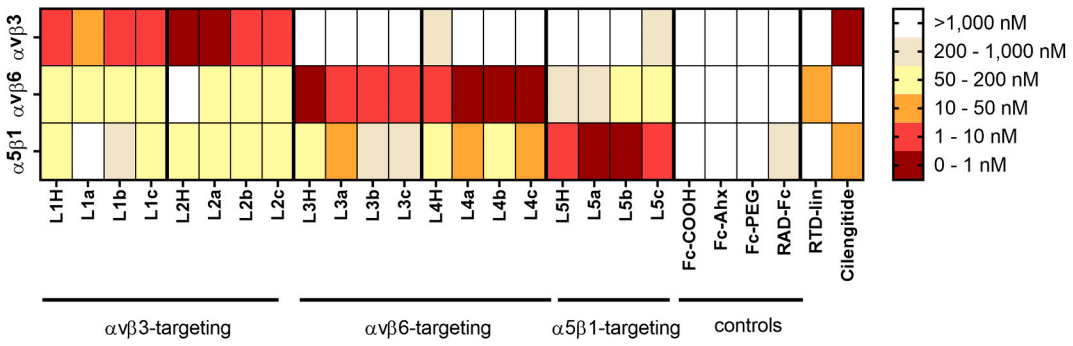

Fig. 2. Heatmap of binding affinities to immobilized integrins determined by ELISA. Displayed are IC_{50} values in nM of unconjugated integrin ligands L1H-L5H, Fc-derivatives L1a-L5c, negative controls Fc-COOH, Fc-Ahx, Fc-$(PEG)_2$, RAD-Fc, and standards RTD-lin and Cilengitide for αvβ3, αvβ6, and α5β1, respectively. The corresponding IC_{50}-values and method description are given in Table 1.

We could not detect a negative effect of Fc conjugation on αvβ3-affinity of L1-and L2-based ligands, indicating that Fc did not sterically hinder integrin binding. However, we noticed changes in selectivity of L1 and L2-based ligands after Fc-conjugation.

For example, L1a-c lost affinity towards $\alpha 5\beta 1$ (91 to1000 nM) compared to L1H (55 nM) but maintained αvβ6 affinity similar to its parent ligand L1H. In contrast, the peptidomimetic αvβ3-targeting ILFs L2a-c displayed increased affinity to both αvβ6 and α5β1, thus being less selective. This effect was most pronounced for αvβ6, where the binding affinity of L2H (>1000 nM) increased to 114–146 nM in L2a-c. The other ligands (L3, L4, L5 and L6-based ligands) all showed no affinity to αvβ3 (IC_{50} >1000 nM), with the exception of L4H and L5c, which showed a very low, but measurable affinity around 350 nM. The αvβ6 targeting L3-based ILFs L3b and L3c showed a low nanomolar affinity of 9.5 and 1.2 nM to αvβ6, albeit slightly lower compared to L3H (IC_{50}: 0.3 nM). At the same time, their α5β1 binding affinity decreased from 73 nM (L3H) to 251 nM and 283 nM, respectively. The L4 derivatives L4a and L4c showed subnanomolar affinities to αvβ6 (IC_{50}: 0.08 and 0.23 nM, respectively), compared to 1.3 nM of L4H and showed increased α5β1 affinity (36 and 27 nM, respectively vs. 105 nM). Neither of the L3-and L4-based ligands showed affinity to αvβ3. Of note, L4a-c (αvβ6) and L5a-b (α5β1) showed subnanomolar affinity to their respective integrins, compared to low nanomolar affinity of their parent ligands L4H and L5H. To our knowledge, L5a and L5b represent two of the best α5β1 binding peptidomimetic derivatives so far reported. Non-integrin targeted controls (Fc-COOH, Fc-Ahx, Fc-$(PEG)_2$, RAD-Fc) indicated no binding affinity at all to either integrin subtype.

Overall, we can assert that conjugation type a (no linker) and b (Ahx-linker) displayed better affinity/selectivity profiles than type c ($(PEG)_2$-linker) ligands. Importantly, we were able to identify ILFs harboring high affinity and selectivity for each integrin subtype.

3.3. *Determination of the integrin expression profile of a panel of cancer cell lines*

For *in vitro* testing of ILF performance, we identified a panel of human cancer cell lines including melanoma (M21 [54–57] and the subline M21-L [55–58]), oral squamous cell carcinoma (HN [49,59] and

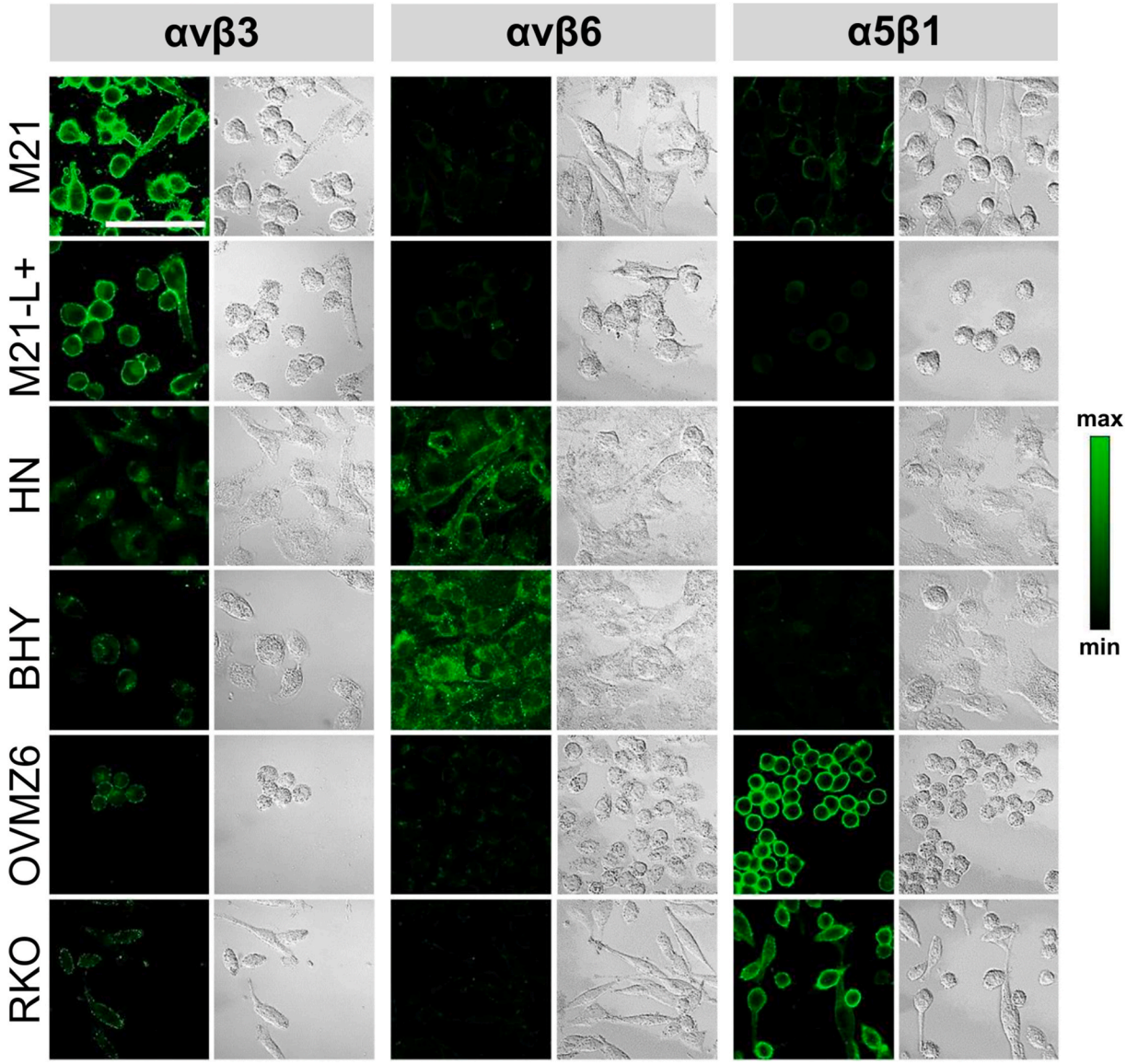

Fig. 3. Immunofluorescence detection of integrins αvβ3, α5β1, and αvβ6. Cell immunostaining using primary antibodies against αvβ3, α5β1, or αvβ6, followed by a secondary Alexa 568-conjugated goat-anti-mouse IgG antibody. Fluorescence images and corresponding differential interference contrast (DIC) images were obtained using a confocal laser-scanning microscope (LSM510, Zeiss, Jena). Scale bar: 50 μm.

BHY [49,59]), colon carcinoma (RKO [60]), and ovarian cancer (OV-MZ-6 [49,61,62]) cells, and characterized their distinct expression profile of αvβ3, αvβ6, and α5β1 by immunocytochemical (ICC) staining (Fig. 3). We found that αvβ3 expression was highest in M21 cells and low to non-detectable in RKO, OV-MZ-6, HN, and BHY, respectively. M21-L, a subline of M21, established by Cheresh et al. as low to negative for αvβ3 expression [63], displayed weak, but clearly detectable αvβ3 staining. This indicates that the subline slightly regained its capacity to express the αvβ3 heterodimer. In order to take this into consideration, we here defined the subline as M21-L+. Expression of αvβ6 was highest in HN cells, followed by BHY cells, while only very low αvβ6 levels were observed in M21, M21-L+, RKO or OV-MZ-6 cells. OV-MZ-6 and RKO cells showed high α5β1 expression with only minor levels detected in M21, M21-L+, HN, and BHY cells. Unspecific binding of the secondary antibody was controlled by staining procedures in the absence of the primary antibody and was negligible (Figure S48). In summary, for each of the three investigated integrins, we identified two cell lines that predominantly expressed one integrin subtype with low to non-detectable levels of the other two integrins ($\alpha v\beta 3^+$: M21, M21-L+; $\alpha v\beta 6^+$: HN, BHY; $\alpha 5\beta 1^+$: OV-MZ-6, RKO), allowing monitoring of ILF integrin subtype selectivity.

3.4. Cytotoxic effects of ILF-derivatives

In order to assess the therapeutic potential of integrin-mediated Fc delivery, we assayed the cytotoxic potential of the synthesized ILFs via MTT assays. We determined the concentration leading to 50% cell viability within 24 h in dose-response experiments ranging between 0 and 1000 μM ILF. Data were analyzed via non-linear regression. We termed this value GI_{50} (growth inhibition 50%) to avoid confusion with IC_{50}, which we used for the affinity of the compounds. The GI_{50} values are displayed in Table 2 and the corresponding non-linear regression curves can be found in Figures S49-54. For clarity, the data were further plotted as heatmaps (Fig. 4). We compared the ILF cytotoxicity to that of the parent ligands (L1H-L5H), Fc controls (Fc-COOH, Fc-Ahx, Fc-$(PEG)_2$, RAD-Fc), and cisplatin. Cisplatin is a metal-based chemotherapeutic and the most commonly used reference compound for Fc-containing drugs. Using cisplatin as a positive control in cell viability tests is important, since GI_{50} or IC_{50} determination can produce vastly different values based on the applied methodology and the experimental set-up, such as variations in drug incubation time and post-incubation periods. Here, we used a rather short incubation time of 24 h and no post-incubation time, a protocol likely to produce lower GI_{50} values compared to a 72 h incubation of the same compounds. Relating the obtained GI_{50}-values to cisplatin allowed us to evaluate the potency of our ILF compounds, despite different modes of action that lead to cell death [64–66]. In our study, cisplatin showed potent cytotoxicity expressed in GI_{50} values between 17 and 81 μM in the six tested cancer cell lines, underlining its cytotoxic potency and non-selectivity for different cell types.

Free Fc-COOH showed only very weak effects on cell viability ($GI_{50} > 500\ \mu M$), which confirmed previous data by others and its inefficiency as a drug in its free form [32,33]. Importantly, the parent integrin ligands (devoid of Fc) also exhibited negligible effects on cell viability (GI_{50}: 300–1000 μM), except for the αvβ3-selective ligand L2H, which displayed a slightly reduced cell viability in BHY ($\alpha v\beta 6^+$) and OV-MZ-6 ($\alpha 5\beta 1^+$) cells (GI_{50}: 137 and 217 μM, respectively). Hence, the components we used to create ILFs did not show relevant cytotoxicity against the studied tumor cell lines harboring elevated expression levels of distinct integrin species.

Subsequently, we analyzed the cytotoxic potential of ILFs. The αvβ3-targeting ILFs L1a-c and L2a-c exerted potent anti-tumor activity (GI_{50} values: 30–45 μM) in M21 cells harboring high αvβ3 expression levels, followed by lower αvβ3-expressing M21-L+ cells (GI_{50}: 35–85 μM). In contrast, we observed moderate to low activity in the αvβ3-low expressing cell lines HN, BHY, RKO, and OV-MZ-6 (GI_{50} values: 62–713 μM). Importantly, L1-and L2-based ILFs displayed IC_{50}-values in the

Table 2
Antiproliferative activity (GI_{50} values) in μM of unconjugated integrin ligands L1H-L5H (grey), ILF derivatives L1a-L5c, positive control cisplatin and negative controls Fc-COOH, Fc-Ahx, Fc-$(PEG)_2$, and RAD-Fc on the human cancer cell lines M21, M21-L+, OV-MZ-6, RKO, HN, and BHY. Cells were treated for 24 h and subsequently subjected to an MTT assay. GI_{50} values were calculated using GraphPad Prism 8 and are displayed as mean of three independent experiments and 95% confidence interval.

	$\alpha v\beta 3^+$		$\alpha 5\beta 1^+$		$\alpha v\beta 6^+$	
Compound	M21	M21-L+	OV-MZ-6	RKO	HN	BHY
αvβ3-selective ligands						
L1H	423 (301 … 593)	818 (520 … 1324)	644 (527 … 789)	943 (759 … 1184)	>1000	>1000
L1a	35 (27 … 44)	55 (32 … 91)	237 (147 … 383)	133 (96 … 185)	224 (129 … 383)	287 (147 … 550)
L1b	44 (38 … 50)	84 (43 … 159)	268 (132 … 527)	63 (37 … 103)	121 (72 … 202)	122 (63 … 235)
L1c	37 (25 … 53)	61 (37 … 100)	333 (225 … 491)	73 (51 … 103)	212 (147 … 305)	149 (98 … 227)
L2H	686 (422 … 1138)	>1000	239 (194 … 295)	345 (228 … 520)	549 (338 … 893)	164 (121 … 221)
L2a	45 (37 … 54)	47 (40 … 56)	152 (96 … 240)	77 (55 … 105)	90 (65 … 124)	139 (78 … 246)
L2b	31 (23 … 43)	56 (50 … 63)	233 (100 … 527)	117 (67 … 201)	413 (231 … 736)	713 (487 … 1061)
L2c	35 (28 … 43)	37 (31 … 44)	324 (173 … 597)	102 (74 … 140)	191 (125 … 292)	153 (85 … 276)
αvβ6-selective ligands						
L3H	>1000	>1000	>1000	>1000	>1000	>1000
L3a	864 (502 … 1556)	823 (491 … 1427)	795 (473 … 1382)	398 (275 … 577)	96.0 (67 … 136)	50 (26 … 94)
L3b	>1000	>1000	555 (357 … 869)	152 (98.5 … 234)	27 (21 … 34)	36 (31 … 41)
L3c	852 (619 … 1193)	779 (584 … 1052)	568 (305 … 1066)	185 (130 … 263)	40 (32 … 49)	45 (36 … 57)
L4H	397 (341 … 463)	657 (463 … 979)	467 (335 … 671)	>1000	866 (640 … 1227)	>1000
L4a	582 (429 … 817)	451 (334 … 624)	773 (503 … 1296)	953 (762 … 1222)	131 (101 … 169)	160 (108 … 241)
L4b	240 (204 … 285)	247 (210 … 291)	226 (182 … 284)	514 (377 … 722)	87 (45 … 162)	179 (137 … 234)
L4c	231 (193 … 278)	280 (221 … 357)	493 (398 … 618)	984 (840 … 1169)	48 (33 … 66)	99 (71 … 136)
α5β1-selective						
L5H	418 (190 … 912)	>1000	406 (109 … 137)	>1000	>1000	>1000
L5a	237 (128 … 432)	596 (382 … 940)	47 (24 … 86)	47 (27 … 76)	834 (579 … 1228)	845 (556 … 1318)
L5b	202 (135 … 301)	451 (252 … 809)	89 (79 … 100)	106 (38 … 281)	310 (150 … 626)	166 (111 … 245)
L5c	132 (97 … 179)	653 (359 … 1215)	39 (31 … 47.4)	33.7 (26 … 43)	131 (69 … 248)	258 (206 … 322)
controls						
Cisplatin	17 (13 … 22)	82 (55 … 123)	37 (33 … 42)	18 (0.6 … 63)	37 (23 … 61)	55 (45 … 67)
Fc-COOH						>1000

(continued on next page)

Table 2 (*continued*)

	αvβ3$^+$		α5β1$^+$		αvβ6$^+$	
Compound	M21	M21-L+	OV-MZ-6	RKO	HN	BHY
	513 (393 … 672)	841 (631 … 1136)	567 (314 … 1045)	594 (407 … 877)	788 (455 … 1419)	
Fc-Ahx	>1000	>1000	>1000	>1000	>1000	>1000
Fc-$(PEG)_2$	>1000	>1000	>1000	887 (381 … 2360)	>1000	>1000
RAD-Fc	796 (512 … 1267)	>1000	>1000	>1000	>1000	>1000

mid-affinity range of 50–200 nM to integrins *αvβ6* and α5β1 (compare Fig. 2, Table 1). Therefore, integrin mediated Fc-delivery likely also occurred, although to a lower extent, to αvβ6-and α5β1-overexpressing cell lines during treatment with up to 1000 μM of the tested compound, causing the observed cytotoxic effects.

Overall, L2b (Ahx-linker) showed the best selectivity profile among the αvβ3-targeting ILFs, by displaying the most favorable combination of a potent cytotoxic effect on αvβ3$^+$ M21 and M21-L+ cells and low impact on the viability of the other tumor cell lines.

The αvβ6-targeting ILFs L3a-c and L4a-c showed selective cytotoxicity limited to αvβ6-expressing HN and BHY cells, but L3-based ILF ligands showed markedly higher efficacy than L4-based ligands. This was somehow unexpected since L4-based ILFs displayed higher affinities than L3-based ligands (Fig. 2, Table 1). The compounds L3b (Ahx linker) and L3c ($(PEG)_2$ linker) displayed GI_{50} values between 25 and 45 μM and demonstrated a better cell targeting than L3a, which had GI_{50} values of 50–100 μM in HN and BHY cells. Among the L4-based ligands, L4c showed moderate efficacy with GI_{50} values between 50 and 150 μM in HN and BHY cells, while L4a and L4b were less cytotoxic. M21 and M21-L+ (αvβ3$^+$) as well as RKO and OV-MZ-6 (*α5β1*$^+$) cell viability was not affected by treatment with αvβ6-targeted ILFs. Within this ILF group, L3b was most potent against αvβ6$^+$ cells and was more cytotoxic than cisplatin in HN and BHY cell lines.

L5-based ILFs displayed heterogeneous patterns of cytotoxicity. L5c ($(PEG)_2$-linker) was most potent against *α5β1*$^+$ RKO cells (GI_{50}: 34 μM) and OV-MZ-6 cells (GI_{50}: 39 μM), but also least selective, with moderate efficacy against αvβ6$^+$ HN cells (GI_{50}: 131 μM) and αvβ6$^+$ M21 cells (GI_{50}: 132 μM). L5b was less potent against α5β1$^+$ cells (GI_{50}: 89–106 μM). Collectively, L5a showed the best combination of selective α5β1-targeting (GI_{50}: 47 μM in RKO and OV-MZ-6 cells) with markedly lower cytotoxic effects in the other cells (GI_{50}: 238–845 μM).

In summary, while non-targeted Fc-COOH and integrin ligands alone did not provoke cytotoxic effects, the bioconjugation of Fc-COOH to integrin ligands strongly increased its cytotoxic potential in the presence of the target integrin on the cell membrane up to 30-fold.

Overall, ligands L2b and L2c (αvβ3-targeting, $GI_{50} < 35$ μM for M21 cells) and ligands L3b and L3c (αvβ6-targeting, $GI_{50} < 40$ μM for HN cells) demonstrated the most efficacious integrin subtype-dependent cytotoxicity obtained through targeted Fc delivery. Regarding the α5β1-targeting ILFs, L5a displayed the best compromise between α5β1-dependent cytotoxicity and integrin selectivity. The most potent ligands showed cytotoxicity in the range of or slightly better than cisplatin, but only in tumor cells overexpressing the targeted integrin subtype, while cisplatin is highly effective in killing rapidly proliferating cells.

The only other study that describes targeting of Fc via RGD-peptides [34] is difficult to compare to our results for several reasons. As mentioned, neither the tripeptide RGD used in that study was characterized towards its affinity and integrin subtype selectivity nor the B16 cell model with respect to its specific integrin expression profile. Furthermore, cisplatin was not used as reference for the cell killing potential of RGD-Fc. To our surprise, Zhou et al. reported IC_{50}-values (equivalent to GI_{50}) of 50 μM for Fc-COOH and 20 μM for RGD (without Fc) on B16 cells after 6 h of incubation. These high IC_{50} values of free Fc-COOH and RGD alone are in contrast to our own data, where Fc-COOH was >10-fold less cytotoxic, and investigations by others [32, 33]. The most potent RGD-Fc compound showed an IC_{50}-value of 5 μM, which represents a 10- or 4-fold increase compared to Fc-COOH and RGD. In contrast, in our study, treatment with the ILF L3b resulted in an up to 30-fold increased activity compared to Fc-COOH in HN cells and even higher ratios in BHY cells, where Fc-COOH displayed a GI_{50}-values >1000 μM.

3.5. Cellular uptake of integrin ligands

Prompted by the results provided by MTT assays, we investigated how the ligands with the most potent and selective cytotoxicity profiles (L2b, L3b, L5a) interacted with cells having different integrin expression patterns. In order to enable microscopic evaluation of cell binding and uptake, we synthesized the Cy5.5-conjugated ligands L2-Cy5.5 (αvβ3-targeting), L3-Cy5.5 (αvβ6-targeting), and L5-Cy5.5 (α5β1-targeting) and evaluated their uptake in M21 (αvβ3$^+$), HN (αvβ6$^+$) and OV-MZ-6 (α5β1$^+$) cells, respectively (Fig. 5a). We incubated the cells for 40 min with the Cy5.5-labeled ligands (1 μM), followed by nuclear counterstaining and confocal laser scanning microscopy (CLSM) (Fig. 5b).

As expected, L2-Cy5.5 (αvβ3-targeting) showed the highest uptake

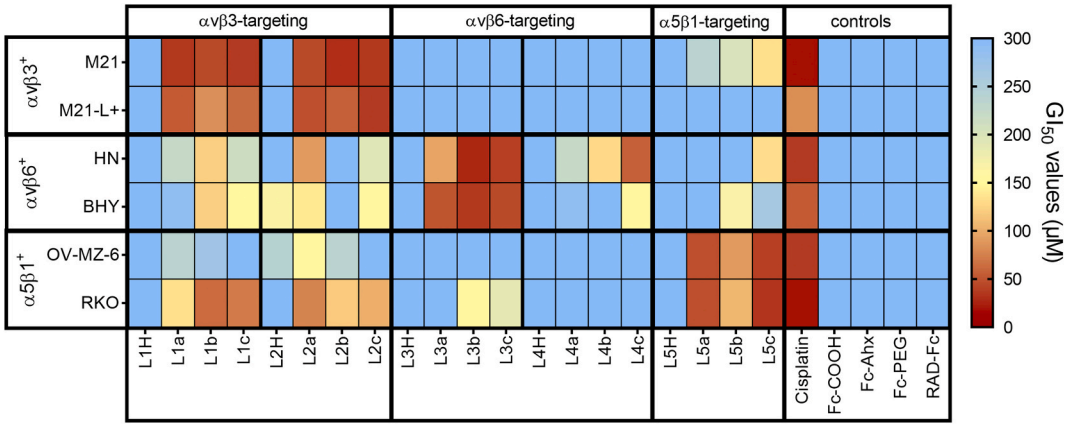

Fig. 4. Cell viability assessment after treatment with ILFs and controls. M21, M21-L+, HN, BHY, OV-MZ-6 and RKO cells were treated with 0–1000 μM of ILF ligands, unconjugated integrin ligands (L1H-L5H), or controls for 24 h. Cell viability was assessed by MTT assay and normalized to untreated cells. Dose-response curves were analyzed via non-linear regression to compute GI_{50}-values (50% growth inhibition), represented here as heatmap. All assays were performed in triplicate with a minimum of three independent experiments. The corresponding GI_{50} values and 95% confidence intervals are given in Table 2.

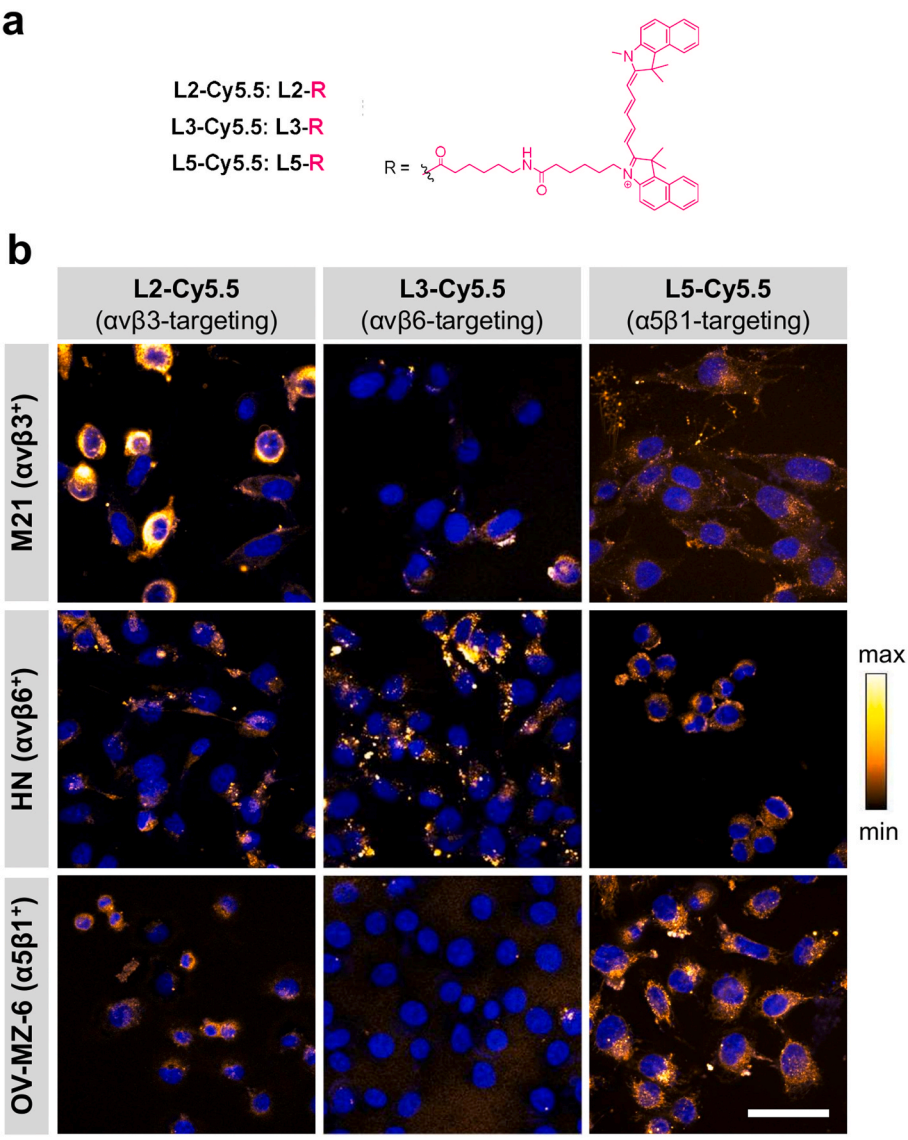

Fig. 5. Cellular uptake of Cy5.5-labeled ligands into cell lines with distinct integrin expression profiles. (a) Structure of Cy5.5, which was conjugated to ligands L2H, L3H and L5H via standard peptide chemistry. **(b)** CLSM imaging of cellular binding and uptake of Cy5.5-labeled integrin ligands. Cells were incubated with 1 μM of L2-Cy5.5, L3-Cy5.5 or L5-Cy5.5 for 40 min Cy5.5 signal is displayed as look-up table orange-to-white. Nuclei were co-stained with Hoechst 33342 (blue signal). Scale bar: 50 μm.

levels into M21 cells, however this compound was also internalized to a lower extent by HN and OV-MZ-6 cells (Fig. 5b). This supported our observation that L2-based ILFs also exerted low to moderate cytotoxicity in these cell lines based on both low-level endogenous αvβ3 expression in all cell lines, as well as a low affinity of L2-based ligands to αvβ6 and α5β1. Importantly, the intracellular distribution of L2-Cy5.5 was in line with the αvβ3 expression pattern determined via ICC (Fig. 6a). In particular, we detected fluorescence signals most prominently at the cell migration front and at cellular protrusions, which are known to be actin- and integrin-rich regions [67]. Together, our data indicate a predominantly αvβ3-specific uptake mechanism of L2-based ligands and confirm the potential for integrin subtype-dependent Fc delivery.

For the αvβ6-targeting L3-Cy5.5, we observed a strong uptake into αvβ6$^+$ HN cells, but not into M21 and OV-MZ-6 cells (Fig. 5b). This underlined the excellent selectivity of L3-based ILFs determined via ELISA and cytotoxicity evaluation. Comparing the pattern of fluorescence signal distribution, it was conspicuous that L3-Cy5.5 produced a dotted pattern in αvβ6$^+$ HN cells. Strikingly, a similar dotted pattern was noticed upon ICC using an αvβ6-directed antibody, supporting that the binding of L3-Cy5.5 reflected the actual cellular αvβ6 distribution (Fig. 6b).

For L5-Cy5.5, the highest cellular uptake was displayed by α5β1$^+$ OV-MZ-6 cells. However, we also detected considerable uptake by HN cells, and low uptake into M21 cells. This uptake behavior was in agreement with ILF cytotoxicity, where L5b and L5c also caused moderate cytotoxic effects on M21 and HN cells.

Thus, cellular uptake patterns of Cy5.5-labeled ligands corresponded well with the cytotoxic effects of the respective ILFs, but differed in some cases from the uptake behavior expected from affinity/integrin expression data. L3-based ligands were the most selective across experiments, with the lowest uptake and cytotoxic effects on cells lacking αvβ6-expression. Although conjugation of a bulky dye to a relatively small peptide or peptidomimetic bears the risk of affecting the binding properties of the conjugates, our data indicate that the uptake of the Cy5.5 labeled ligands mirrored the integrin distribution assessed via antibody staining.

3.6. Fc-mediated ROS production and DNA damage induction

The ILFs showing the best cellular uptake behavior, namely L2b (αvβ3-targeting) and L3b (αvβ6-targeting), were selected to further investigate whether integrin-mediated Fc delivery effectively triggered the observed cell death. Since Fc is a postulated ROS generator, we assessed ROS levels and DNA damage (via γH2AX foci formation) after treatment of M21 cells (αvβ3$^+$) with L2H and L2b, HN cells (αvβ6$^+$) with L3H and L3b, and OV-MZ-6 cells (αvβ3$^-$ and αvβ6$^-$) with L2b and L3b

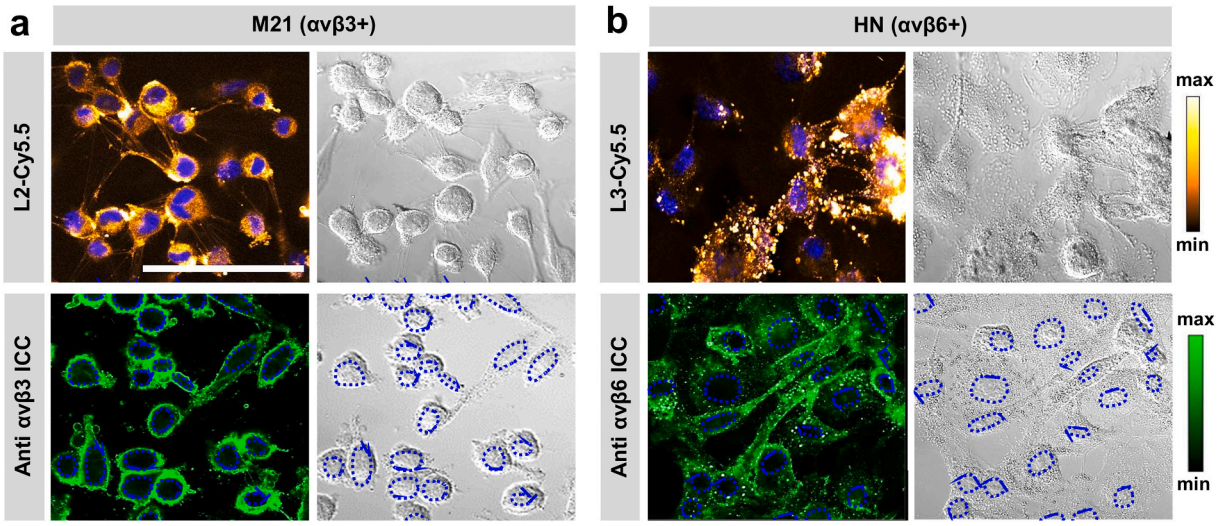

Fig. 6. Comparison of integrin staining via ICC and Cy5.5-labeled integrin ligand uptake. (a) M21 (**a**) and HN (**b**) cells were stained with 1 μM L2-Cy5.5 or L3-Cy5.5, respectively, to evaluate integrin ligand uptake (top row, orange-to-white signal). Integrin expression was determined using either αvβ3 or αvβ3 primary antibody and an AF568-labeled secondary antibody (bottom row; green signal). Displayed are fluorescent and differential interference contrast (DIC) images. Top row: Nucleus counterstained with Hoechst 33342. Bottom row: Nucleus outlined in DIC images. Scale bar: 100 μm.

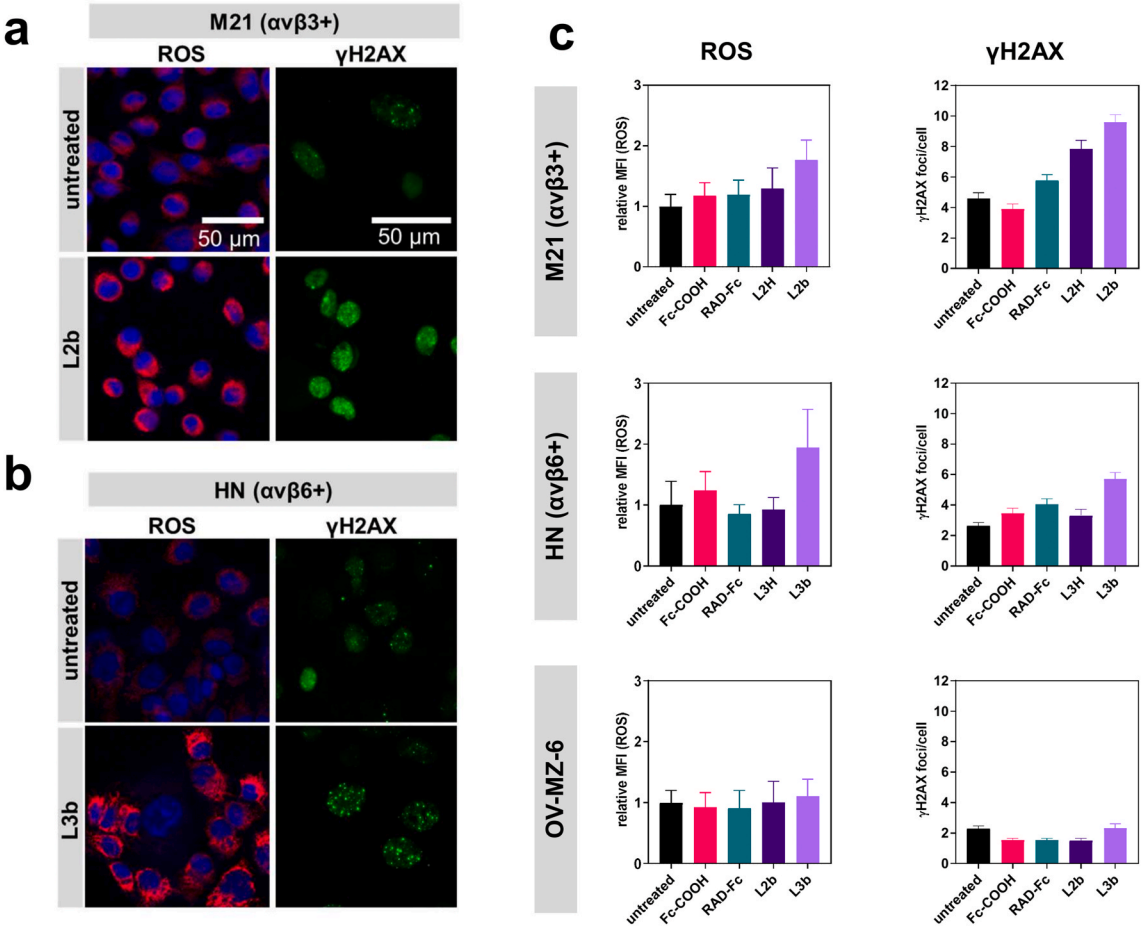

Fig. 7. Detection of ROS production and DNA damage (γH2AX foci) in M21, HN, and OV-MZ-6 cells upon treatment with ILF. Cells were treated for 24 h with 20 μM of either ILF ligands L2b (αvβ3-targeting), L3b (αvβ6-targeting), L2H, L3H, Fc-COOH, or RAD-Fc, respectively. Examples from **(a)** M21 ($\alpha v\beta 3^{+}$) and **(b)** HN cells ($\alpha v\beta 6^{+}$) are shown. ROS were detected using CellROX (red signal) and DNA damage was detected through antibody staining of γH2AX foci (green signal). Nuclei were counterstained with Hoechst 33342 (blue signal). (**c**) Quantification of ROS levels and γH2AX foci. ROS levels were quantified as mean fluorescence intensity per cell and normalized to untreated cells using FIJI. Bars depict mean and standard deviation. γH2AX foci count was determined using the CellProfiler Software. Bars depict mean and standard error of 235 ± 51 cells per condition.

(Fig. 7). In addition, Fc-COOH and RAD-Fc were used as controls on all cell lines.

We detected the highest ROS-levels and number of γH2AX foci/cell in $\alpha v\beta 3^{+}$ M21 cells treated with αvβ3-targeting L2b and $\alpha v\beta 6^{+}$ HN cells treated with αvβ6-targeting L3b (Fig. 7). This was in excellent agreement with the cytotoxicity evaluation (Table 2). In addition, L2b and L3b did not trigger ROS production or γH2AX foci formation in $\alpha 5\beta 1^{+}$ ($\alpha v\beta 3^{-}$, $\alpha v\beta 6^{-}$) OV-MZ-6 cells (Fig. 7c).

Overall, L3b demonstrated the most promising characteristics for future *in vivo* evaluation in mouse models. A preliminary assessment of its serum stability revealed that L3b was stable at 37 °C for 24 h, rendering it suitable for intravenous delivery to tumors (Figures S55-56 and Supplementary Table ST1).

In summary, at equimolar concentrations, Fc delivery via an integrin ligand triggered a much stronger increase in ROS levels, DNA damage, and cell death than free Fc. Our data indicate that active uptake and cellular retention of ILFs play an important role in mediating Fc-mediated anti-tumor effects. Hence, our results are complementary to the approach of incorporating Fc into bioactive molecules, which have been shown to enhance anti-tumor, anti-fungal, and anti-malarial effects [21–25,28,68]. However, in our approach, we focused on the use of per se therapeutically inactive ligand vehicles for Fc-delivery, enhancing its intracellular accumulation in tumor cells expressing the known tumor biomarkers αvβ3, αvβ6, or α5β1. In this regard, the integrin subtype selectivity granted by optimized integrin ligands represents the key element that makes it possible to address specific tumor entities harboring the respective integrin expression profile. It also enables to target different tumor-associated cells within a single tumor, such as angiogenic endothelial cells expressing e.g. high levels of αvβ3.

Importantly, targeted Fc delivery has the potential to increase the therapeutic window by reducing the exposure of non-tumor cells to the cytotoxic treatment upon systemic administration. In that regard, it is important to note that integrins are ubiquitously expressed at a low level in many cell types within the human body. However, our results compellingly support that ILFs successfully induced cytotoxicity only in cells overexpressing the target integrin, but did not affect cells expressing low, endogenous levels of the respective integrin species.

The logical next step will be to evaluate ILFs in *in vivo* treatment studies. Importantly, the peptides and peptidomimetics our ILFs are based on, were previously shown to have suitable characteristics for *in vivo* application. They were particularly evaluated by us and others in molecular imaging studies using radiolabeled agents based on L1 [69–74], L2 [46], L3 [75], L4 [76] and L5 [46,77,78]. Those studies showed the ability of the respective ligands to selectively and specifically accumulate in tumors (preclinical and clinical) that express the targeted integrin subtype, which is an important prerequisite for *in vivo* Fc delivery via ILFs.

4. Conclusions

In this work, we explored the first integrin-subtype selective peptidic and peptidomimetic integrin-ferrocence ligands (ILFs), targeted to the tumor-biologically relevant integrins αvβ3, αvβ6, or α5β1. The most promising ILFs against αvβ3 (L2b) and αvβ6 (L3b) showed excellent integrin-dependent Fc-mediated cytotoxicity, which correlated well with increased ROS levels and induced DNA damage. ILFs were up to 30-fold more cytotoxic than free Fc at equimolar concentrations. Thus, we were able to develop integrin ligands as promising vehicles for tumor-targeted therapy via delivering the ROS generator Fc into cancer cells. This approach has the potential to maximize anti-cancer efficacy and minimize systemic toxicity, thereby improving the therapeutic window of Fc compared to currently used non-selective anti-cancer drugs.

Declaration of competing interest

The authors declare that they have no known competing financial interests or personal relationships that could have appeared to influence the work reported in this paper.

Acknowledgements

We would like to thank the Core Facility for NMR and LC-MS at the Department of Chemistry at the TU Munich, Garching, and the Cell Analysis Core Facility of *TranslaTUM* at the Klinikum rechts der Isar, Munich. We also thank Birgit Blechert and Sandra Sühnel for technical support during *in vitro* experiments. We thank Paul H. Weinreb and Shelia Violette from Biogen for kind provision of the αvβ6 directed antibody clone 6.2A1 [40]. Furthermore, we thank Prof. Dr. Wolfgang A. Weber and PD Dr. Johannes Notni for helpful discussions.

Appendix A. Supplementary data

Supplementary data related to this article can be found at https://doi.org/10.1016/j.biomaterials.2021.120754.

Funding

S. T. acknowledges MIUR, PON R&I 2014-2020-AIM (Attraction and International Mobility), project AIM1873131-2, linea 1. L.M., S.D.M., F·S.D.L. acknowledge MIUR, PRIN 2017PHRC8X. L.M. and F·S.D.L. acknowledge Regione Campania – POR Campania FESR 2014/2020, B61G18000470007. H.K. received funding from the Deutsche Forschungsgemeinschaft (DFG) (Ke 147/42–1).

Data availability statement

The authors declare that all data supporting the findings of this study are available within the paper and its supplementary information files. The associated raw data and step-by-step protocols can be made available from the corresponding author upon reasonable request.

Credit author statement

Beatrice Stefanie Ludwig: Conceptualization, Investigation, Methodology Formal analysis, Validation, Data curation, Writing – original draft, Writing – review & editing; Stefano Tomassi: Writing – review & editing, Data curation, Methodology; Salvatore Di Maro: Writing – review & editing, Data curation; Methodology; Francesco Saverio Di Leva: Writing – review & editing, Data curation; Methodology; Anke Benge: Methodology, Investigation; Florian Reichart: Methodology. Markus Nieberler: Writing – review & editing, Resources; Fritz E. Kühn: Supervision, Writing – review & editing, Resources; Horst Kessler: Writing – review & editing, Methodology, Resources; Luciana Marinelli: Supervision, Writing – review & editing, Data curation, Resources; Ute Reuning: Conceptualization, Visualization, Supervision, Data curation, Writing – original draft, Writing – review & editing, Resources; Susanne Kossatz: Conceptualization, Visualization, Supervision, Data curation, Writing – original draft, Writing – review & editing, Resources, Software

References

[1] T.M. Allen, Ligand-targeted therapeutics in anticancer therapy, Nat. Rev. Canc. 2 (2002) 750–763.
[2] C. Sawyers, Targeted cancer therapy, Nature 432 (2004) 294–297.
[3] K. Ley, J. Rivera-Nieves, W.J. Sandborn, S. Shattil, Integrin-based therapeutics: biological basis, clinical use and new drugs, Nat. Rev. Drug Discov. 15 (2016) 173–183.
[4] M. Nieberler, et al., Exploring the role of RGD-recognizing integrins in cancer, Cancers 9 (2017).
[5] E. Ruoslahti, M.D. Pierschbacher, New perspectives in cell adhesion: RGD and integrins, Science 238 (1987) 491.
[6] R.O. Hynes, Integrins: bidirectional, allosteric signaling machines, Cell 110 (2002) 673–687.
[7] M. Barczyk, S. Carracedo, D. Gullberg, Integrins. *Cell Tissue Res* 339 (2010) 269–280.

[8] R.O. Hynes, Integrins: versatility, modulation, and signaling in cell adhesion, Cell 69 (1992) 11–25.
[9] F.G. Giancotti, E. Ruoslahti, Integrin signaling, Science 285 (1999) 1028.
[10] M.D. Pierschbacher, E. Ruoslahti, Variants of the cell recognition site of fibronectin that retain attachment-promoting activity, Proc. Natl. Acad. Sci. Unit. States Am. 81 (1984) 5985.
[11] J.S. Desgrosellier, D.A. Cheresh, Integrins in cancer: biological implications and therapeutic opportunities, Nat. Rev. Canc. 10 (2010) 9–22.
[12] M. Nieberler, et al., Exploring the role of RGD-recognizing integrins in cancer, Cancers 9 (2017) 116.
[13] C.L. Gladson, S. Hancock, M.M. Arnold, O.M. Faye-Petersen, R.P. Castleberry, D. R. Kelly, Stage-specific expression of integrin alphaVbeta3 in neuroblastic tumors, Am. J. Pathol. 148 (1996) 1423–1434.
[14] R. Huang, E.K. Rofstad, Integrins as therapeutic targets in the organ-specific metastasis of human malignant melanoma, J. Exp. Clin. Canc. Res. 37 (2018).
[15] J. Roman, J.D. Ritzenthaler, S. Roser-Page, X. Sun, S. Han, α5β1-Integrin expression is essential for tumor progression in experimental lung cancer, Am. J. Respir. Cell Mol. Biol. 43 (2010) 684–691.
[16] G. Renner, et al., Integrin alpha 5 beta 1 and p53 convergent pathways in the control of anti-apoptotic proteins PEA-15 and survivin in high-grade glioma, Cell Death Differ. 23 (2016) 640–653.
[17] H. Janouskova, et al., Integrin alpha 5 beta 1 plays a critical role in resistance to temozolomide by interfering with the p53 pathway in high-grade glioma, Canc. Res. 72 (2012) 3463–3470.
[18] T.J. Kealy, P.L. Pauson, A new type of organo-iron compound, Nature 168 (1951) 1039–1040.
[19] S.A. Miller, J.A. Tebboth, J.F. Tremaine, 114. Dicyclopentadienyliron, J. Chem. Soc. (1952) 632–635.
[20] G. Wilkinson, M. Rosenblum, M.C. Whiting, R.B. Woodward, The structure OF iron BIS-cyclopentadienyl, J. Am. Chem. Soc. 74 (1952) 2125–2126.
[21] M. Patra, G. Gasser, The medicinal chemistry of ferrocene and its derivatives, Nat Rev Chem 1 (2017), 0066.
[22] B.S. Ludwig, J.D.G. Correia, F.E. Kühn, Ferrocene derivatives as anti-infective agents, Coord. Chem. Rev. 396 (2019) 22–48.
[23] B. Albada, N. Metzler-Nolte, Organometallic–peptide bioconjugates: synthetic strategies and medicinal applications, Chem. Rev. 116 (2016) 11797–11839.
[24] R. Wang, H.H. Chen, W.T. Yan, M.W. Zheng, T.S. Zhang, Y.H. Zhang, Ferrocene-containing hybrids as potential anticancer agents: current developments, mechanisms of action and structure-activity relationships, Eur. J. Med. Chem. 190 (2020).
[25] C. Ornelas, Application of ferrocene and its derivatives in cancer research, New J. Chem. 35 (2011) 1973–1985.
[26] G. Jaouen, A. Vessières, S. Top, Ferrocifen type anti cancer drugs, Chem. Soc. Rev. 44 (2015) 8802–8817.
[27] M. Barends, A. Jaidee, N. Khaohirun, P. Singhasivanon, F. Nosten, In vitro activity of ferroquine (SSR 97193) against Plasmodium falciparum isolates from the Thai-Burmese border, Malar. J. 6 (2007) 81.
[28] K. Kowalski, Recent developments in the chemistry of ferrocenyl secondary natural product conjugates, Coord. Chem. Rev. 366 (2018) 91–108.
[29] F. Noor, R. Kinscherf, G.A. Bonaterra, S. Walczak, S. Wölfl, N. Metzler-Nolte, Enhanced cellular uptake and cytotoxicity studies of organometallic bioconjugates of the NLS peptide in hep G2 cells, Chembiochem 10 (2009) 493–502.
[30] P. Kovacic, Unifying mechanism for anticancer agents involving electron transfer and oxidative stress: clinical implications, Med. Hypotheses 69 (2007) 510–516.
[31] M.H. Raza, et al., ROS-modulated therapeutic approaches in cancer treatment, J. Canc. Res. Clin. Oncol. 143 (2017) 1789–1809.
[32] R.A. Yeary, Chronic toxicity of dicyclopentadienyliron (ferrocene) in dogs, Toxicol. Appl. Pharmacol. 15 (1969) 666–&.
[33] Z. Miklan, R. Szabo, V. Zsoldos-Mady, J. Remenyi, Z. Banoczi, F. Hudecz, New ferrocene containing peptide conjugates: synthesis and effect on human leukemia (HL-60) cells, Biopolymers 88 (2007) 108–114.
[34] B. Zhou, J. Li, B.J. Feng, Y. Ouyang, Y.N. Liu, F. Zhou, Syntheses and in vitro antitumor activities of ferrocene-conjugated Arg-Gly-Asp peptides, J. Inorg. Biochem. 116 (2012) 19–25.
[35] T.G. Kapp, M. Fottner, O.V. Maltsev, H. Kessler, Small cause, great impact: modification of the guanidine group in the RGD motif controls integrin subtype selectivity, Angew Chem. Int. Ed. Engl. 55 (2016) 1540–1543.
[36] T.G. Kapp, et al., A comprehensive evaluation of the activity and selectivity profile of ligands for RGD-binding integrins, Sci. Rep. 7 (2017) 39805.
[37] C. Mas-Moruno, F. Rechenmacher, Kessler H. Cilengitide, The first anti-angiogenic small molecule drug candidate design, synthesis and clinical evaluation, Anticancer Agents Med Chem 10 (2010) 753–768.
[38] S. Kraft, B. Diefenbach, R. Mehta, A. Jonczyk, G.A. Luckenbach, S.L. Goodman, Definition of an unexpected ligand recognition motif for alphav beta6 integrin, J. Biol. Chem. 274 (1999) 1979–1985.
[39] V. Möbus, R. Kreienberg, R. Moll, C. Gerharz, Establishment and characterization of 6 human ovarian-cancer cell lines, Arch. Gynecol. Obstet. 242 (1987) 457–458.
[40] P.H. Weinreb, et al., Function-blocking integrin alpha(v)beta(6) monoclonal antibodies - distinct ligand-mimetic and nonligand-mimetic classes, J. Biol. Chem. 279 (2004) 17875–17887.
[41] M.E. Mercurio, et al., Switchable protecting strategy for solid phase synthesis of DNA and RNA interacting nucleopeptides, J. Org. Chem. 81 (2016) 11612–11625.
[42] M. Aumailley, M. Gurrath, G. Müller, J. Calvete, R. Timpl, H. Kessler, Arg-Gly-Asp constrained within cyclic pentapeptides. Strong and selective inhibitors of cell adhesion to vitronectin and laminin fragment P1, FEBS Lett. 291 (1991) 50–54.
[43] R. Haubner, R. Gratias, B. Diefenbach, S.L. Goodman, A. Jonczyk, H. Kessler, Structural and functional aspects of RGD-containing cyclic pentapeptides as highly potent and selective integrin αVβ3 antagonists, J. Am. Chem. Soc. 118 (1996) 7461–7472.
[44] M. Pfaff, et al., Selective recognition of cyclic RGD peptides of NMR defined conformation by alpha IIb beta 3, alpha V beta 3, and alpha 5 beta 1 integrins, J. Biol. Chem. 269 (1994) 20233–20238.
[45] R. Haubner, D. Finsinger, H. Kessler, Stereoisomeric peptide libraries and peptidomimetics for designing selective inhibitors of the αvβ3 integrin for a new cancer therapy, Angew Chem. Int. Ed. Engl. 36 (1997) 1374–1389.
[46] S. Neubauer, et al., Selective imaging of the angiogenic relevant integrins α5β1 and αvβ3, Angew Chem. Int. Ed. Engl. 52 (2013) 11656–11659.
[47] S. Neubauer, et al., Pharmacophoric modifications lead to superpotent αvβ3 integrin ligands with suppressed α5β1 activity, J. Med. Chem. 57 (2014) 3410–3417.
[48] F. Rechenmacher, et al., Functionalizing αvβ3- or α5β1-selective integrin antagonists for surface coating: a method to discriminate integrin subtypes in vitro, Angew Chem. Int. Ed. Engl. 52 (2013) 1572–1575.
[49] O.V. Maltsev, et al., Stable peptides instead of stapled peptides: highly potent αvβ6-selective integrin ligands, Angew Chem. Int. Ed. Engl. 55 (2016) 1535–1539.
[50] F.S. DiLeva, et al., From a helix to a small cycle: metadynamics-inspired αvβ6 integrin selective ligands, Angew. Chem. Int. Ed. 57 (2018) 14645–14649.
[51] D. Heckmann, A. Meyer, B. Laufer, G. Zahn, R. Stragies, H. Kessler, Rational design of highly active and selective ligands for the α5β1 integrin receptor, Chembiochem 9 (2008) 1397–1407.
[52] S.I. Kirin, F. Noor, N. Metzler-Nolte, W. Mier, Manual solid–phase peptide synthesis of metallocene–peptide bioconjugates, J Chem Educ 84 (2007) 108.
[53] A.O. Frank, et al., Conformational control of integrin-subtype selectivity in isoDGR peptide motifs: a biological switch, Angew Chem. Int. Ed. Engl. 49 (2010) 9278–9281.
[54] D.A. Cheresh, R. Pytela, M.D. Pierschbacher, F.G. Klier, E. Ruoslahti, R.A. Reisfeld, An Arg-Gly-Asp-directed receptor on the surface of human melanoma cells exists in an divalent cation-dependent functional complex with the disialoganglioside GD2, J. Cell Biol. 105 (1987) 1163–1173.
[55] I.F. Charo, L. Nannizzi, J.W. Smith, D.A. Cheresh, The vitronectin receptor alpha v beta 3 binds fibronectin and acts in concert with alpha 5 beta 1 in promoting cellular attachment and spreading on fibronectin, J. Cell Biol. 111 (1990) 2795–2800.
[56] B. Felding-Habermann, B.M. Mueller, C.A. Romerdahl, D.A. Cheresh, Involvement of integrin alpha V gene expression in human melanoma tumorigenicity, J. Clin. Invest. 89 (1992) 2018–2022.
[57] D.A. Cheresh, R.C. Spiro, Biosynthetic and functional properties of an Arg-Gly-Asp-directed receptor involved in human melanoma cell attachment to vitronectin, fibrinogen, and von Willebrand factor, J. Biol. Chem. 262 (1987) 17703–17711.
[58] P. Lanza, B. Felding-Habermann, Z.M. Ruggeri, M. Zanetti, R. Billetta, Selective interaction of a conformationally-constrained arg-gly- asp (RGD) motif with the integrin receptor αvβ3 expressed on human tumor cells, Blood Cells Mol. Dis. 23 (1997) 230–241.
[59] H. Kawamata, K. Nakashiro, D. Uchida, K. Harada, H. Yoshida, M. Sato, Possible contribution of active MMP2 to lymph-node metastasis and secreted cathepsin L to bone invasion of newly established human oral-squamous-cancer cell lines, Int. J. Canc. 70 (1997) 120–127.
[60] D. Boyd, G. Florent, P. Kim, M. Brattain, Determination of the levels of urokinase and its receptor in human colon carcinoma cell lines, Canc. Res. 48 (1988) 3112–3116.
[61] M.A. Müller, et al., The glycophorin A transmembrane sequence within integrin αvβ3 creates a non-signaling integrin with low basal affinity that is strongly adhesive under force, J. Mol. Biol. 425 (2013) 2988–3006.
[62] S. Hapke, et al., Ovarian cancer cell proliferation and motility is induced by engagement of integrin alpha(v)beta3/Vitronectin interaction, Biol. Chem. 384 (2003) 1073–1083.
[63] D.A. Cheresh, R.C. Spiro, Biosynthetic and functional-properties of an arg-gly-asp-directed receptor involved in human-melanoma cell attachment to vitronectin, fibrinogen, and vonwillebrand-factor, J. Biol. Chem. 262 (1987) 17703–17711.
[64] L. Astolfi, et al., Correlation of adverse effects of cisplatin administration in patients affected by solid tumours: a retrospective evaluation, Oncol. Rep. 29 (2013) 1285–1292.
[65] E.M. Blanchard, Cisplatin and solid tumors: still working, after all these years, J. Solid Tumors 2 (2011) 26–33.
[66] G. Ciarimbola, Membrane transporters as mediators of cisplatin side-effects, Anticancer Res. 34 (2014) 547–550.
[67] P.K. Mattila, P. Lappalainen, Filopodia: molecular architecture and cellular functions, Nat. Rev. Mol. Cell Biol. 9 (2008) 446–454.
[68] C.G. Hartinger, N. Metzler-Nolte, P.J. Dyson, Challenges and opportunities in the development of organometallic anticancer drugs, Organometallics 31 (2012) 5677–5685.
[69] R. Haubner, F. Bruchertseifer, M. Bock, H. Kessler, M. Schwaiger, H. Wester, Synthesis and biological evaluation of a Tc-99m-labelled cyclic RGD pepticle for imaging the alpha v beta 3 expression, Nuklearmed-Nucl Med 43 (2004) 26–32.
[70] R. Haubner, et al., [F-18]Galacto-RGD: synthesis, radiolabeling, metabolic stability, and radiation dose estimates, Bioconjugate Chem. 15 (2004) 61–69.
[71] R. Haubner, et al., Noninvasive visualization of the activated alpha v beta 3 integrin in cancer patients by positron emission tomography and [F-18]Galacto-RGD, PLoS Med. 2 (2005) 244–252.
[72] R. Haubner, et al., Radiolabeled alpha(v)beta(3) integrin antagonists: a new class of tracers for tumor targeting, J. Nucl. Med. 40 (1999) 1061–1071.

[73] R. Haubner, et al., Noninvasive imaging of alpha(v)beta(3) integrin expression using F-18-labeled RGD-containing glycopeptide and positron emission tomography, Canc. Res. 61 (2001) 1781–1785.
[74] I. Laitinen, et al., Comparison of cyclic RGD peptides for alpha(v)beta(3) integrin detection in a rat model of myocardial infarction, EJNMMI Res. 3 (2013).
[75] A.J. Beer, et al., Non-invasive assessment of inter-and intrapatient variability of integrin expression in metastasized prostate cancer by PET, Oncotarget 7 (2016) 28151–28159.
[76] N.G. Quigley, et al., Click-chemistry (CuAAC) trimerization of an alpha(v)beta(6) integrin targeting Ga-68-Peptide: enhanced contrast for in-vivo PET imaging of human lung adenocarcinoma xenografts, Chembiochem 21 (2020) 2836–2843.
[77] C. D'Alessandria, et al., In vivo biokinetic and metabolic characterization of the Ga-68-labelled alpha 5 beta 1-selective peptidomimetic FR366, Eur. J. Nucl. Med. Mol. Imag. 43 (2016) 953–963.
[78] J. Notni, et al., Complementary, selective PET imaging of integrin subtypes alpha (5)beta(1) and alpha(v)beta(3) using Ga-68-Aquibeprin and Ga-68-Avebetrin, J. Nucl. Med. 57 (2016) 460–466.
[79] M.A. Dechantsreiter, et al., N-methylated cyclic RGD peptides as highly active and selective alpha(v)beta(3) integrin antagonists, J. Med. Chem. 42 (1999) 3033–3040.